Chemical Engineering Journal 225 (2013) 16–24

Contents lists available at SciVerse ScienceDirect

Chemical Engineering Journal

journal homepage: www.elsevier.com/locate/cej

Sulfite oxidation in seawater flue gas desulfurization by plate falling film corona-streamer discharge

Xiaoping Wang, Zhongjian Li, Tian Lan, Lecheng Lei *

Key Laboratory of Biomass Chemical Engineering of Ministry of Education, Department of Chemical and Biological Engineering, Zhejiang University, Hangzhou 310027, China

HIGHLIGHTS

- Tried to use plate falling film discharge to solve the scale-up problem of electric discharge reactor.
- Preliminarily discussed the mechanism of sulfite oxidation by electrical discharge.
- Found that the discharge power density is the dominating factor of sulfite oxidation rate.
- Simplified the kinetic model in terms of sulfite concentration and power density.

ARTICLE INFO

Article history:
Received 23 November 2012
Received in revised form 22 February 2013
Accepted 20 March 2013
Available online 27 March 2013

Keywords:
Sulfite oxidation
Plate falling film discharge
Power density
Kinetic equation
Scale-up

ABSTRACT

In this paper, sulfite containing effluent from the packed tower of seawater flue gas desulfurization is treated by plate falling film corona-streamer discharge which can solve the scale-up problem of electrical discharge reactors. Effects of pH, electrical discharge intensity, effluent flow rate and temperature on sulfite oxidation are considered. Experimental results indicate that discharge power density is the dominating factor which affects the sulfite oxidation rate by affecting the gaseous radical concentration. Based on experimental results, sulfite oxidation by corona-streamer discharge is proposed as the combination of chain reaction path and radical self-reaction path. In addition, the simplified kinetic equation is expressed in terms of sulfite concentration and discharge power density. Comparing with cylindrical falling film corona-streamer discharge, the plate falling film corona-streamer discharge leads to a fold increase in energy efficiency, besides, scale-up of a plate falling film corona-streamer discharge reactor will affect the energy efficiency insignificantly, all these indicate that the plate falling film discharge has a better potential in large scale utilization than cylindrical falling film discharge.

1. Introduction

Seawater flue gas desulfurization (SWFGD) is a promising approach to control SO_2 emission from power plants. A typical SWFGD process consists of three steps [1,2]: (1) absorbing SO_2 with seawater in a packed tower, (2) diluting the effluent with fresh seawater and aerating oxidation of sulfite (S(IV)), and (3) adjusting the pH to over 6.8 with fresh seawater. After these three steps, the effluent can be discharged into the sea. Compared with other flue gas desulfurization technologies, simple treatment of sulfite containing effluent is the most important advantage for SWFGD.

Although SWFGD is a promising technology, it still has some drawbacks in application. The aeration oxidation rate of S(IV) is limited by effluent pH. Vidal et al. has pointed out that the aeration oxidation of S(IV) hardly proceeds at low pH (2–4) [3], which is around the pH of effluent from the packed tower. Thus, a huge amount of fresh seawater is needed to increase the effluent pH before aeration oxidation, which results in a large aeration basin and high power consumption. To minimize the size and power consumption of the oxidation basin, the effluent should be treated without dilution. To raise the S(IV) oxidation rate, using catalysts like activated carbon and metal ions has been proved to be an efficient way [1,4–6]. However, catalyst separation and regeneration processes are needed, otherwise the exhausted catalysts may become pollutants in seawater.

Besides using catalysts, non-thermal plasma generated by high voltage electrical discharge can be an alternative approach. Restricted by the high conductivity of seawater, water surface discharge is more suitable than electrohydraulic discharge. Typical water surface discharge reactors suspend high voltage (HV) electrodes above water surface and put ground electrodes in water [7]. The discharge occurs in the air and on the air–water interface. Studies on characteristics of water surface discharge have been carried out in many works [8–15]. Our previous work has preliminarily

* Corresponding author. Tel./fax: +86 57187952525.
E-mail address: lablei@zju.edu.cn (L. Lei).

1385-8947/$ - see front matter © 2013 Elsevier B.V. All rights reserved.
http://dx.doi.org/10.1016/j.cej.2013.03.084

Nomenclature

A	pre-exponential factor of the Arrhenius equation
$C_{S(IV)}$	sulfite concentration in the effluent, mol/ L
C_{O2}	dissolved O_2 concentration, mol/L
C_{Ri}	liquid phase radical concentrations, mol/L
$C_{S(IV),0}$	inlet sulfite concentration, mol/L
$C_{S(IV),p}$	outlet sulfite concentration, mol/L
$C_{S(IV),t}$	sulfite concentration at the operation time of t, mol/L
d	discharge gap distance, cm
E_a	activation energy, J/mol
E_p	pulsed electric field, kV/cm
f	pulsed repetition frequency, Hz
G	energy efficiency, mol/J
I	current, A
k	reaction rate constant with electrical discharge
$k_1 - k_{14}$	reaction rate constants of the chain reaction, $dm^3\ mol^{-1}\ s^{-1}$
k_i	reaction rate constants with respect to different radicals
$k_{S(IV)}$	reaction rate constant
K	empirical reaction rate constant
L	length of cylindrical discharge gap, cm
m	reaction order with respect to sulfite
n	reaction order with respect to radical
P	discharge power, W
P_d	power density, W/ cm^3
r_i	radius of the HV electrode, cm
r_o	inner radius of the outer tube, cm
$r_{S(IV)}$	reaction rate of sulfite
R	gas constant, J/(kmol)
S	area of the ACF felt, cm^2
S_c	effective area of cylindrical falling film, cm^2/cm^3
S_p	effective area of plate falling film, cm^2/cm^3
t	operation time, s
t_p	duration time of a pulse, s
T	Kelvin temperature, K
U	voltage, V
V_E	volume of treated effluent, L
V_p	peak voltage, kV
α	reaction order with respect to S(IV) concentration
α_i	reaction orders with respect to sulfite concentration
β	reaction order with respect to O_2 concentration
β_i	reaction orders with respect to different radicals
ε	radical generation coefficient by electrical discharge
$\gamma_{S(IV)}$	sulfite conversion per pass
η	Henry coefficient of the radical

discussed the effect of cylindrical falling film discharge on S(IV) oxidation [16], results of which show that the reaction rate is significantly accelerated by cylindrical falling film discharge especially at low pH.

However, scale-up of the cylindrical falling film discharge reactor is difficult. Due to the coaxial arrangement of the HV electrode and the cylindrical ground electrode, the effective area of electrical discharge plasma decreases with the increase of outer tube radius. In addition, the electric field also decreases as the outer tube radius increases. Thus, scale-up of the cylindrical falling film discharge reactor can only be achieved by building higher reactors. Otherwise the decreases of effective area and electric field will cause the decrease of energy efficiency. This problem can be solved by using plate falling film discharge. The parallel arrangement of electrodes keeps the effective area and the electric field constant when increasing the surface area of falling film. Thus, this paper investigates the behavior of plate falling film corona-streamer discharge on S(IV) oxidation. Effects of some important operation factors are discussed. Based on experimental results, the reaction mechanism and reaction kinetic equation are deduced.

2. Experimental

2.1. Experimental setup

The power supply used is the same as that used in our previous work [16]. Schematic circuit of the pulsed power supply is shown in Fig. 1. The maximum output is 70 kV with a pulse width of about 500 ns and a rise time of about 100 ns. The repetition frequency can be adjusted from 10 to 200 pulse per second (pps). In this paper, experiments are conducted at the constant repetition frequency of 100 pps.

Structure of the falling film discharge system is shown in Fig. 2. The HV electrode was made of activated carbon fiber (ACF) felt with a size of 8.5 × 8.5 cm and the ground electrode was made of graphite plate with a size of 10 × 10 cm. The distance between the HV electrode and the ground electrode can be adjusted from 3 mm to 15 mm. ACF felt is a kind of porous carbon composed of activated carbon fibers. Fiber tips on the surface make it a natural multi-needle system. Because of the large quantity and uniform distribution of fiber tips, it is more likely to form large scale uniform plasma in the inter-electrode space in comparison with artificial multi-needle systems.

The effluent stored in the water tank was pumped into the overflow tank to form a falling film on the graphite plate. After flowing through the discharge gap, the product stream flows back to the water tank. The effluent flow rate was controlled by a flowmeter. The effluent temperature was maintained by a thermostatic water bath and can be adjusted from 283 K to 373 K.

2.2. Artificial effluent

The artificial effluent was prepared by dissolving $NaHSO_3$ in the artificial seawater. The formula of artificial seawater listed in Table 1 is the combination of the McClendon formula, the Subow formula, and the Lyman and Fleming formula [17]. Minor components like NaBr, H_3BO_3, Na_2SiO_3, Al_2Cl_6 and so on were not added, which influenced the total saltness little. The pH was adjusted by NaOH

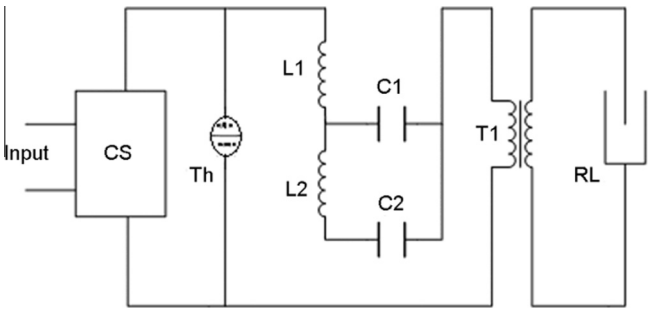

Fig. 1. Schematic circuit of the pulsed power supply. Input: A.C.220V; CS: Constant high-voltage high-frequency resonant charging system; L_1, L_2: resonant inductors; C_1, C_2: high voltage capacitors; Th: hydrogen thyratron; T_1: high voltage transformer; RL: reactor load.

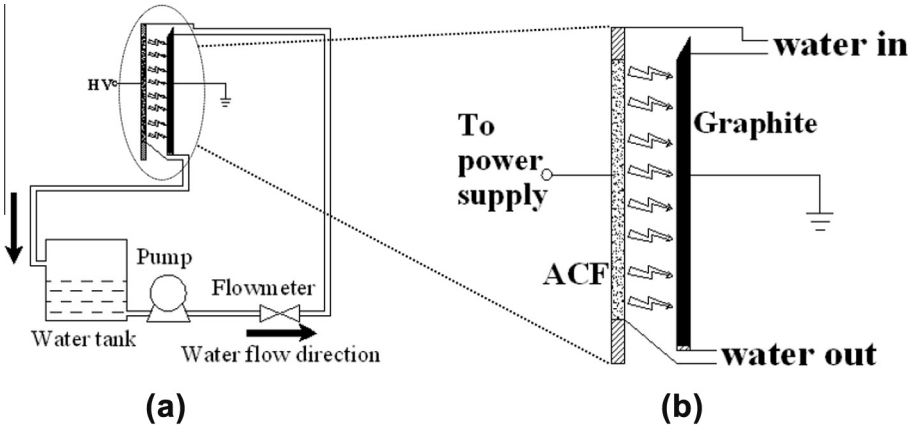

Fig. 2. Experimental setup: (a) the experimental system, and (b) the falling film discharge reactor.

Table 1
Formula of the artificial seawater.

Compound	Concentration (g/L)
NaCl	26.75
$MgCl_2$	4.88
$MgSO_4$	3.54
KCl	0.72
$CaCl_2$	1.16

solution and HCl solution. The concentration of $NaHSO_3$ was changed from 0.3 mM to 2.5 mM to cover the S(IV) concentration of effluent from the packed tower.

2.3. Experimental procedure

2.3.1. Experimental factors

For our reaction system, the S(IV) oxidation reaction rate was affected by factors including the discharge intensity, the solution condition, the flow rate and the operation temperature.

The change of discharge intensity was obtained by changing the electric field and the power density. To maintain the corona-streamer discharge, the electric field was chosen from 12 kV/cm to 19 kV/cm and the power density was chosen from 0.02 W/cm^3 to 0.15 W/cm^3. The changes of electric field and discharge power density were obtained by changing the supplied voltage and the discharge gap distance.

For S(IV) oxidation, the dominating solution condition which significantly affects the oxidation rate is pH. In this paper, the initial pH was chosen from 3 to 5, in which the pH of S(IV) containing effluent from the packed tower was covered.

Chosen of the effluent flow rate should assure that the ground electrode can be fully covered by falling film and no turbulence occurred. In this paper, the effluent flow rate can be chosen from 15 L/h to 25 L/h.

The actual temperature of the effluent from the packed tower is larger than the room temperature. To cover the potential effluent temperature, the experimental effluent temperature was changed from 285 K to 325 K.

For each experiment, two replications were conducted to validate the experimental result.

2.3.2. Sampling and analysis

Water samples were taken from the water tank by a pipette. Before test, the water sample was diluted from 1 mL to 50 mL by distilled water. The S(IV) concentration was tested by an ion chromatography (Dionex ICS 1100, USA) with a AS 18 column (Dionex, USA) and a conductivity detector. The mobile phase was potassium hydroxide solution with a concentration of 23 mM and a flow rate of 1.5 mL/min.

The pulsed voltage and current supplied to the reactor were monitored by a digital oscilloscope (Tektronix DPO 3000, USA) with a 1:1000 high voltage probe (Tektronix P6015A, USA) and a current probe (Tektronix TCP 0150, USA). The optical emission spectrum was measured by a multi-channel spectrometer (Avantes Avaspec 2048-USB2-8, NL). The pH was monitored by a pH meter (Leici PHSJ-3F, China).

3. Results and discussion

3.1. Mechanism of S(IV) oxidation by electrical discharge

The auto-oxidation of S(IV) with oxygen is a chain reaction initiated by radicals, which has been summarized by Buxton et al. as follows [18].

(1) Initiation step

$$\cdot OH + SO_3^{2-} \rightarrow OH^- + SO_3^{-\cdot}, \quad k_1 = 4.6 \times 10^9\ dm^3\ mol^{-1}\ s^{-1} \tag{R1}$$

$$\cdot OH + HSO_3^- \rightarrow H_2O + SO_3^{-\cdot}, \quad k_2 = 2.7 \times 10^9\ dm^3\ mol^{-1}\ s^{-1} \tag{R2}$$

(2) Propagation step

$$SO_3^{-\cdot} + O_2 \rightarrow SO_5^{-\cdot}, \quad k_3 = 2.5 \times 10^9\ dm^3\ mol^{-1}\ s^{-1} \tag{R3}$$

$$SO_5^{-\cdot} + HSO_3^- \rightarrow SO_3^{-\cdot} + HSO_5^-, \quad k_4 = 8.6 \times 10^3\ dm^3\ mol^{-1}\ s^{-1} \tag{R4}$$

$$SO_5^{-\cdot} + SO_3^{2-} \xrightarrow{H^+} HSO_5^- + SO_3^{-\cdot}, \quad k_5 = 2.1 \times 10^5\ dm^3\ mol^{-1}\ s^{-1} \tag{R5}$$

$$SO_5^{-\cdot} + HSO_3^- \rightarrow SO_4^{-\cdot} + SO_4^{2-} + H^+, \quad k_6 = 3.6 \times 10^2\ dm^3\ mol^{-1}\ s^{-1} \tag{R6}$$

$$SO_5^{-\cdot} + SO_3^{2-} \rightarrow SO_4^{-\cdot} + SO_4^{2-}, \quad k_7 = 5.5 \times 10^5\ dm^3\ mol^{-1}\ s^{-1} \tag{R7}$$

$$SO_4^{-\cdot} + HSO_3^- \rightarrow HSO_4^{2-} + SO_3^{-\cdot}, \quad k_8 = 6.8 \times 10^8\ dm^3\ mol^{-1}\ s^{-1} \tag{R8}$$

$$SO_4^{\cdot-} + SO_3^{2-} \rightarrow SO_4^{2-} + SO_3^{\cdot-}, \quad k_9 = 3.1 \times 10^8\ dm^3\ mol^{-1}\ s^{-1} \tag{R9}$$

$$SO_5^{\cdot-} + SO_5^{\cdot-} \rightarrow 2SO_4^{\cdot-} + O_2, \quad k_{10} = 2.2 \times 10^8\ dm^3\ mol^{-1}\ s^{-1} \tag{R10}$$

(3) Termination step

$$SO_3^{\cdot-} + SO_3^{\cdot-} \rightarrow S_2O_6^{2-}, \quad k_{11} = 1.5 \times 10^8\ dm^3\ mol^{-1}\ s^{-1} \tag{R11}$$

$$SO_4^{\cdot-} + SO_4^{\cdot-} \rightarrow S_2O_8^{2-}, \quad k_{12} = 3.1 \times 10^8\ dm^3\ mol^{-1}\ s^{-1} \tag{R12}$$

$$SO_5^{\cdot-} + SO_5^{\cdot-} \rightarrow S_2O_8^{2-} + O_2, \quad k_{13} = 4.5 \times 10^8\ dm^3\ mol^{-1}\ s^{-1} \tag{R13}$$

The overall reaction rate is controlled by propagation reactions including SO_3^{2-} and HSO_3^- oxidation by $SO_5^{\cdot-}$ radicals (R4–R7). The reaction rate constants of SO_3^{2-} oxidation by $SO_5^{\cdot-}$ radicals (k_5 and k_7) are much bigger than that of HSO_3^- oxidation (k_4 and k_6). Since the ratio of HSO_3^-/SO_3^{2-} increases with the decrease of pH, the S(IV) oxidation rate decreases as pH decreases. Thus, the change of S(IV) oxidation rate with pH is an obvious feature of the chain reaction path.

When exposed to electrical discharge plasma, the reaction path may be changed. Electrical discharge increases the hydroxyl radical concentration, which results in the increase of $SO_5^{\cdot-}$ concentration. When the consumption rate of $SO_5^{\cdot-}$ by S(IV) oxidation (R4–R7) is much lower than the generation rate (R1–R3), self-reaction of $SO_5^{\cdot-}$ radicals (R10 and R13) will become noticeable to balance the producing and consuming. $S_2O_8^{2-}$ produced in R13 will be decomposed to SO_4^{2-} and $SO_4^{\cdot-}$ quickly by R14. $SO_4^{\cdot-}$ radicals produced in R10 and R14 will be consumed by S(IV) oxidation reactions shown as R8 and R9. The radical self-reaction path is summarized as follows:

$$\cdot OH + SO_3^{2-} \rightarrow OH^- + SO_3^{\cdot-}, \quad k_1 = 4.6 \times 10^9\ dm^3\ mol^{-1}\ s^{-1} \tag{R1}$$

$$\cdot OH + HSO_3^- \rightarrow H_2O + SO_3^{\cdot-}, \quad k_2 = 2.7 \times 10^9\ dm^3\ mol^{-1}\ s^{-1} \tag{R2}$$

$$SO_3^{\cdot-} + O_2 \rightarrow SO_5^{\cdot-}, \quad k_3 = 2.5 \times 10^9\ dm^3\ mol^{-1}\ s^{-1} \tag{R3}$$

$$SO_5^{\cdot-} + SO_5^{\cdot-} \rightarrow 2SO_4^{\cdot-} + O_2, \quad k_{10} = 2.2 \times 10^8\ dm^3\ mol^{-1}\ s^{-1} \tag{R10}$$

$$SO_5^{\cdot-} + SO_5^{\cdot-} \rightarrow S_2O_8^{2-} + O_2, \quad k_{13} = 4.5 \times 10^8\ dm^3\ mol^{-1}\ s^{-1} \tag{R13}$$

$$S_2O_8^{2-} + e_{aq}^- \rightarrow SO_4^{2-} + SO_4^{\cdot-}, \quad k_{14} = 1.2 \times 10^{10}\ dm^3\ mol^{-1}\ s^{-1} \tag{R14}$$

$$SO_4^{\cdot-} + HSO_3^- \rightarrow HSO_4^{2-} + SO_3^{\cdot-}, \quad k_8 = 6.8 \times 10^8\ dm^3\ mol^{-1}\ s^{-1} \tag{R8}$$

$$SO_4^{\cdot-} + SO_3^{2-} \rightarrow SO_4^{2-} + SO_3^{\cdot-}, \quad k_9 = 3.1 \times 10^8\ dm^3\ mol^{-1}\ s^{-1} \tag{R9}$$

As can be seen, R8 and R9 may be the dominating S(IV) consumption reactions for the radical self-reaction path. Taking into account the same order of reaction rate constants of R8 and R9, the radical self-reaction path will not be affected by pH.

It is discussed above that both the chain reaction path and the radical self-reaction path can be enhanced by electrical discharge. The main difference between these two reaction paths is the sensitivity on pH. The chain reaction rate decreases as pH decreases, while the radical self-reaction path is not affected by pH.

Influence of pH on S(IV) oxidation by plate falling corona-streamer discharge is shown in Fig. 3. The oxidation rate is not affected by initial pH in the range of 3–5. For each initial pH, the instantaneous pH decreases with operation time being the lowest of 2.6, while the S(IV) oxidation rate is almost constant. It means that S(IV) oxidation by electrical discharge is not affected by pH from 2.6 to 5. Thus, it can be supposed that the overall reaction is the combination of chain reaction path and radical self-reaction path and the latter is dominating. Then, the restriction of pH on S(IV) oxidation is eliminated by electrical discharge plasma. This is the superiority of electrical discharge in comparison with catalytic oxidation. Vidal et al. has reported that the catalytic oxidation is affected by pH in a similar way to noncatalytic oxidation, the oxidation rate for pH = 4 is about 3 times higher than that for pH = 3 [4].

3.2. Effect of discharge intensity on S(IV) oxidation

The reaction mechanism revealed above indicates that the S(IV) oxidation rate depends on the discharge intensity. For a ready-made reactor, the discharge intensity is determined by electric field and power density. The pulsed electric field and the discharge power density are calculated by Eqs. (1) and (3) respectively.

$$E_p = \frac{V_p}{d} \tag{1}$$

$$P = f \int_{t_p} UIdt \tag{2}$$

$$P_d = \frac{P}{Sd} \tag{3}$$

where E_p is the pulsed electric field, V_p is the peak voltage, d is the discharge gap distance, P is the discharge power, P_d is the power density, f is the pulsed repetition frequency, U and I are voltage and current respectively, t_p is the duration time of a pulse and S is the area of the ACF felt. It can be found from these three equations that effects of almost all electric and geometrical parameters on

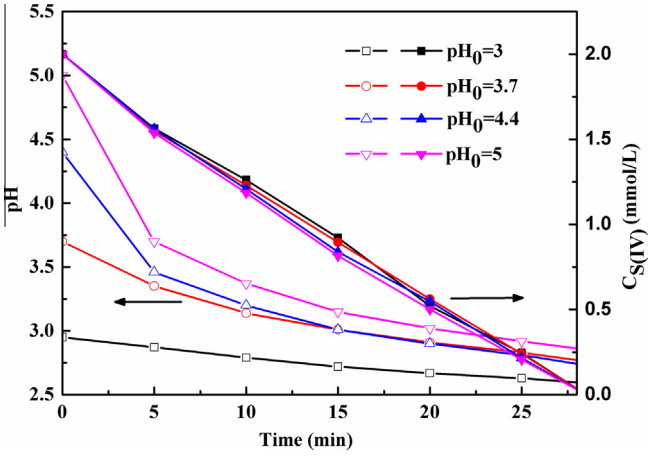

Fig. 3. Effect of pH on S(IV) oxidation rate (T = 283 K, Q = 19.1 L/h, V_p = 15.9 kV, and d = 9.5 mm).

discharge intensity can be attributed to electric field and power density.

3.2.1. Effect of electric field

As shown in Eq. (1), the electric field is determined by the voltage drop between the parallel set electrodes and the gap distance. Effect of electric field on S(IV) oxidation is shown in Fig. 4. In Fig. 4a, the S(IV) oxidation rate increases with electric field. When raising the electric field, the discharge power increases nonlinearly because of the increase of discharge current. The calculated power densities for electric fields of 12.8 kV/cm, 15 kV/cm and 16.7 kV/cm are 0.01 W/cm^3, 0.022 W/cm^3 and 0.109 W/cm^3 respectively, thus, raising the electric field from 15 kV/cm to 16.7 kV/cm obtains a much larger improvement of S(IV) oxidation rate than raising it from 12.8 kV/cm to 15 kV/cm.

When maintaining the electric fields for different gap distances at 16.7 kV/cm, the S(IV) oxidation rate increases with gap distance as shown in Fig. 4b. To maintain the electric field, the discharge power density should be increased as the discharge gap distance increases. The calculated power densities for gap distances of 4.5 mm, 7 mm, 9.5 mm and 14.5 mm are 0.028 W/cm^3, 0.048 W/cm^3, 0.109 W/cm^3 and 0.122 W/cm^3 respectively. It can be found from Fig. 4b that the S(IV) oxidation rate increases with power density even at the constant electric field. Thus, though electric field influences the S(IV) oxidation rate, it is not the dominating factor. If the electric field is large enough to incept the discharge and excite the required radicals, the dominating factor may be the power density. In other word, electric field determines the radical category but not the concentrations.

3.2.2. Effect of power density

Effect of power density on S(IV) oxidation is shown in Fig. 5. In Fig. 5a, the S(IV) oxidation rate increases with power density. When maintaining the power densities for different gap distances at 0.048 W/cm^3, the S(IV) oxidation rate is constant as shown in Fig. 5b. This result implies that the S(IV) oxidation rate is determined by power density in the discharge gap. The reason can be attributed to the effect of power density on gaseous radical concentration, which can be seen from the optical emission spectral (OES).

Radicals generated by electrical discharge have been diagnosed by OES by many researchers [8,19–21]. Optical emission spectrums at different power densities are shown in Fig. 6a and specific emission peaks of typical radicals (including hydroxyl radical (·OH), oxygen radical (·O), ozone (O_3), excited oxygen molecule (O_2^*) and excited nitrogen molecule (N_2^*) are labeled. The intensity of the specific emission peak represents the concentration of the radical. Effect of power density on radical concentration is summarized in Fig. 6b. It can be found that concentrations of all radicals increase with power density linearly.

Two conclusions can be made from Fig. 6b. First, the radical concentration depends on power density. When changing the

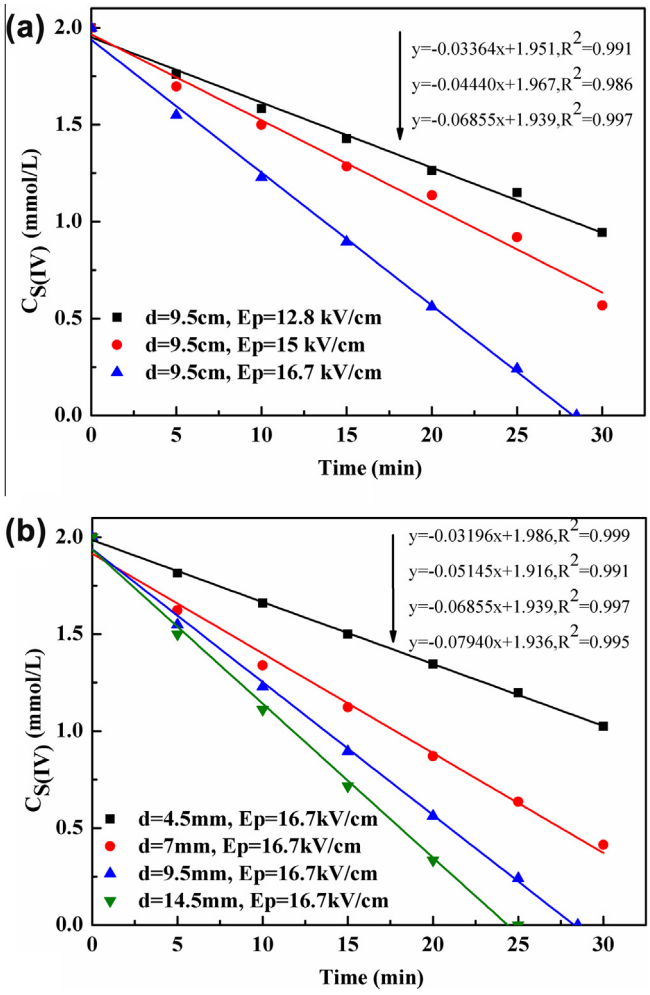

Fig. 4. Effect of electric field on S(IV) oxidation: (a) different electric field, and (b) constant electric field (T = 283 K, Q = 19.1 L/h, and pH_0 = 3).

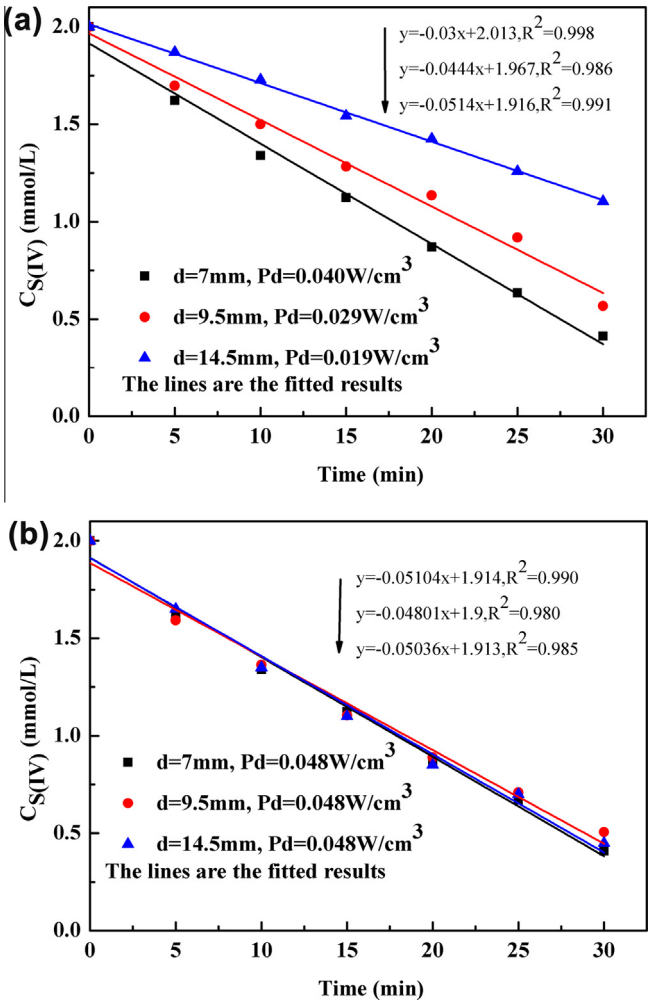

Fig. 5. Dependence of S(IV) oxidation rate on power density: (a) different power density, and (b) constant power density (T = 283 K, Q = 19.1 L/h, and pH_0 = 3).

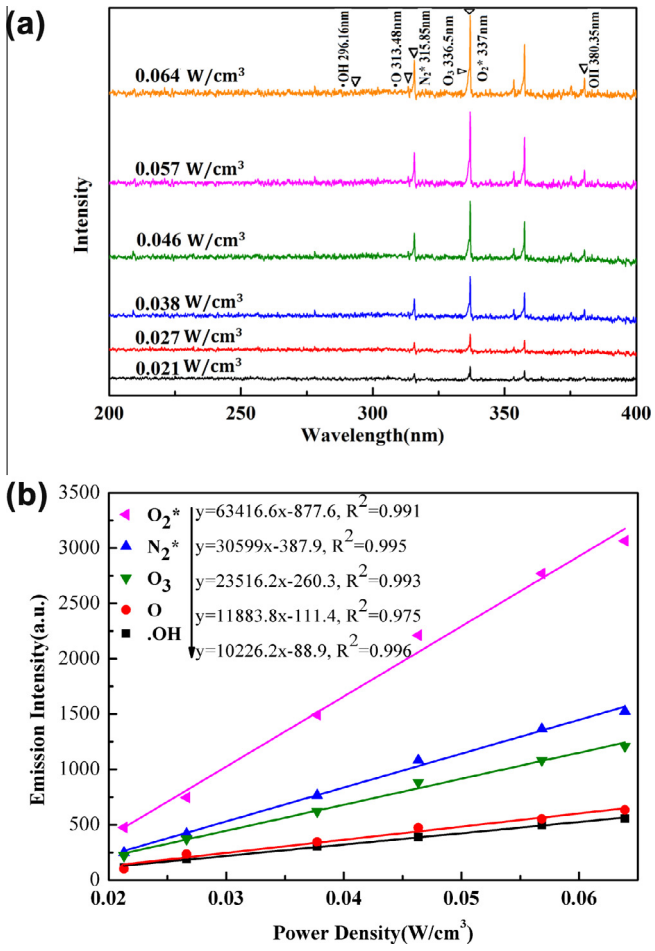

Fig. 6. Dependence of OES on power density: (a) spectrums, and (b) emission intensities (T = 283 K, Q = 19.1 L/h, pH_0 = 3, and d = 9.5 mm).

power density, the radical concentration changes linearly. This conclusion explains the reason why S(IV) oxidation depends on discharge power density.

The second conclusion is that the gaseous radical composition is independent on power density. Because of the linear variation trends, the concentration ratios of all radicals are kept constants when changing the power density. That is to say, the radical concentration in the discharge gap can be expressed by the power density with a coefficient, this supposition agrees with the conclusion obtained by Yan et al. when studying the gaseous reaction of electrical discharge plasma [22,23].

3.3. Kinetic study

The kinetic study of S(IV) oxidation by plate falling film discharge is based on works with respect to aeration oxidation [3], in which the kinetic equation is expressed in the following equation:

$$r_{S(IV)} = -\frac{dC_{S(IV)}}{dt} = k_{S(IV)} C_{S(IV)}^{\alpha} C_{O_2}^{\beta} \quad (4)$$

where $k_{S(IV)}$ is the reaction rate constant, α and β are reaction orders with respect to S(IV) and dissolved O_2 respectively.

The process of S(IV) oxidation by falling film discharge is much more complex than that of aeration oxidation because of many kinds of radicals such as ozone, oxygen radical, hydroxyl radical and hydrogen peroxide produced by electrical discharge. The overall reaction is the combination of all these radicals. So the S(IV) oxidation rate by electrical discharge should be expressed as following:

$$r_{S(IV)} = -\frac{dC_{S(IV)}}{dt} = \sum_i (k_i C_{S(IV)}^{\alpha_i} C_{R_i}^{\beta_i}) \quad (5)$$

In which the subscript i indicates different radicals.

It is difficult to calculate the reaction rate constants and reaction orders in Eq. (5) because of the difficulty to measure the exact concentration of each radical. Some approximate treatment must be conducted to simplify the kinetic equation. All kinds of radicals are simulated by a hypothetical radical. And then, Eq. (5) can be transformed as following:

$$r_{S(IV)} = -\frac{dC_{S(IV)}}{dt} = kC_{S(IV)}^{m} C_{Rl}^{n} \quad (6)$$

In which C_{Rl} represents the radical concentration in the effluent, k is the reaction rate constant, m and n are reaction orders with respect to S(IV) and radical respectively.

The S(IV) conversion per pass is expressed as the following equation:

$$\gamma_{S(IV)} = \frac{C_{S(IV),0} - C_{S(IV),p}}{C_{S(IV),0}} = \frac{\int r_{S(IV)} dt}{C_{S(IV),0}} = \frac{\int kC_{S(IV)}^{m} C_{Rl}^{n} dt}{C_{S(IV),0}} \quad (7)$$

In which $\gamma_{S(IV)}$ is the S(IV) conversion per pass, $C_{S(IV),0}$ and $C_{S(IV),p}$ are the inlet concentration and outlet concentration respectively. Since S(IV) conversion in the short falling film is small, the S(IV) concentration in the film may be considered equal to the inlet concentration approximately. Consequently, S(IV) conversion per pass becomes a power function of the inlet S(IV) concentration,

$$\gamma_{S(IV)} \propto C_{S(IV),0}^{m-1} \quad (8)$$

According to Eq. (8), the reaction order with respect to S(IV) can be evaluated from the slope of ln $\gamma_{S(IV)}$ versus ln $C_{S(IV),0}$.

For experiments conducted at the constant inlet concentration, S(IV) conversion per pass can be expressed as a power function of the radical concentration.

$$\gamma_{S(IV)} \propto C_{Rl}^{n} \quad (9)$$

The reaction order with respect to the radical can be obtained from the slope of ln $\gamma_{S(IV)}$ versus ln C_{Rl}.

3.3.1. Reaction order with respect to S(IV)

Experimental factors except the inlet S(IV) concentration are constants. Evaluation of the reaction order with respect to S(IV) is shown in Fig. 7, in which the slope of ln $\gamma_{S(IV)}$ versus ln $C_{S(IV),0}$ is about −1. According to Eq. (8), the reaction order with respect to S(IV) concentration is about zero. The reason may be that the reaction rate between radicals and S(IV) is very quick. In this case, the apparent S(IV) oxidation rate is determined by the absorption rate of gaseous radicals, as a result, the calculated reaction order with respect S(IV) is zero. It explains the reason why S(IV) oxidation rate is independent on operation time when recycling the product stream.

3.3.2. Reaction order with respect to radical concentration

Radical concentration in the falling film is decided by the corresponding gaseous concentration (C_{Rg}) and the Henry coefficient (η). Thus, Eq. (7) can be rewritten as the following equation:

$$\gamma_{S(IV)} = \frac{\int r_{S(IV)} dt}{C_{S(IV),0}} = \frac{\int kC_{S(IV)}^{m} (\eta C_{Rg})^{n} dt}{C_{S(IV),0}} \quad (10)$$

The gaseous radical concentration can be replaced by the power density with a coefficient.

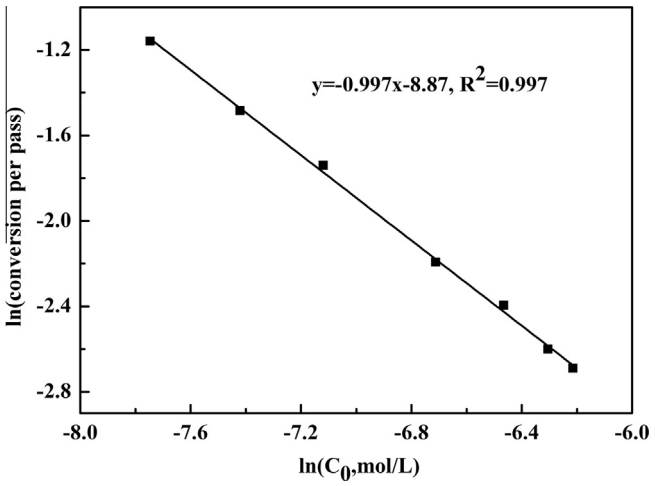

Fig. 7. Evaluation of the reaction order with respect to S(IV) (T = 283 K, Q = 19.1 L/h, pH_0 = 3, d = 9.5 mm, and P_d = 0.087 W/cm^3).

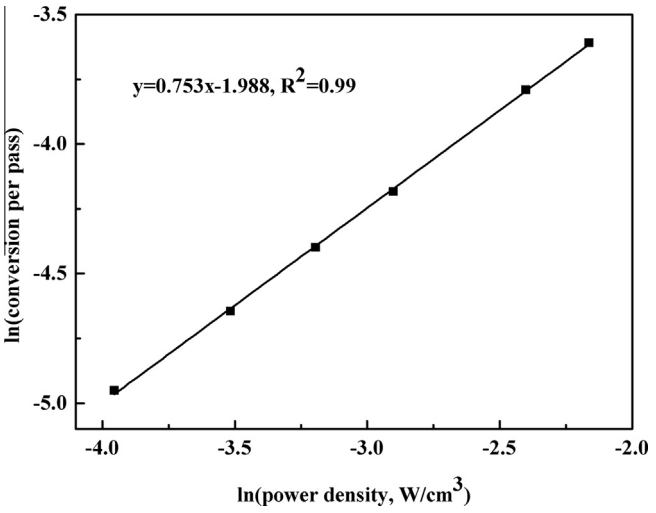

Fig. 8. Evaluation of the reaction order with respect to power density (T = 283 K, Q = 19.1 L/h, pH_0 = 3, d = 9.5 mm, and $C_{S(IV),0}$ = 2 mM).

$$\gamma_{S(IV)} = \frac{\int r_{S(IV)}dt}{C_{S(IV),0}} = \frac{kC_{S(IV)}^{m}(\eta\varepsilon P_d)^{n}dt}{C_{S(IV),0}} \quad (11)$$

In which ε is the radical generation coefficient by electrical discharge.

Thus, the reaction order with respect to radical concentration is equal to that with respect to power density.

Evaluation of the reaction order with respect to power density is shown in Fig. 8. Experimental factors except discharge power density are constants. The slope of ln $\gamma_{S(IV)}$ versus ln P_d is about 0.75. It means that the reaction order with respect to power density is about 0.75. So the kinetic equation of S(IV) oxidation by plate falling film corona-streamer discharge can be written as following:

$$r_{S(IV)} = -\frac{dC_{S(IV)}}{dt} = KP_d^{0.75} \quad (12)$$

in which

$$K = k\eta^{0.75}\varepsilon^{0.75} \quad (13)$$

3.3.3. Temperature dependence of S(IV) oxidation rate

Temperature plays an important role in S(IV) oxidation. Effect of temperature on S(IV) oxidation can be analyzed by the Arrhenius equation expressed as the following equation:

$$\ln\ k = \frac{-E_a}{RT} + \ln\ A \quad (14)$$

In which, E_a is the activation energy, R is the gas constant, T is the Kelvin temperature and A is the pre-exponential factor.

Experiments are conducted at five different effluent temperatures (283, 293, 303, 313 and 323 K). Based on the reaction rate constants obtained at these five temperatures, the ln $K-1/RT$ relation is shown in Fig. 9 in which the slope of ln $K-1/RT$ is -14226. According to the Arrhenius equation, the calculated activation energy is E_a = 14.23 kJ/mol. However, the pre-exponential factor cannot be obtained from Fig. 9, as the coefficients of η and ε are included in the empirical reaction rate constant.

3.4. Effect of effluent flow rate on S(IV) oxidation

Effect of effluent flow rate on S(IV) oxidation is shown in Fig. 10. The oxidation rate increases with effluent flow rate until it exceeding 22.3 L/h, after which the oxidation rate starts to decrease.

Since the product stream is totally recycled to the water tank, the increase of effluent flow rate has little influence on the total amount of absorbed radicals. The slight improvement of S(IV) oxidation is due to the increase of falling film thickness as the flow rate increases, which decreases the discharge gap distance and increases the discharge power density in the discharge gap. When the flow rate continually increases to 22.3 L/h, the uniformity of electrical discharge will be disturbed by turbulence of the falling film [24], which results in the decrease of generation and absorption of gaseous radicals, as a result, the S(IV) oxidation rate begins to decrease.

3.5. Energy efficiency of S(IV) oxidation

To compare the plate falling film discharge with cylindrical falling film discharge, the energy efficiency of S(IV) oxidation is discussed in Fig. 11. The corresponding S(IV) oxidation rates are shown in Fig. 4a. The energy efficiency is defined by the following equation:

$$G = \frac{V_E(C_{S(IV),0} - C_{S(IV),t})}{Pt} \quad (15)$$

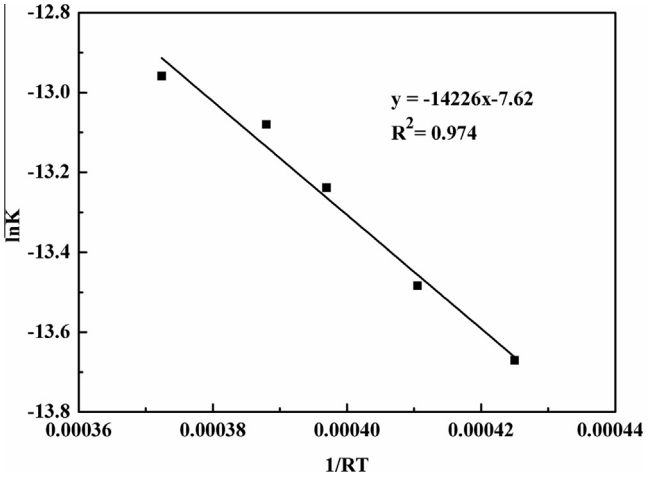

Fig. 9. Temperature dependence of S(IV) oxidation rate (Q = 19.1 L/h, pH_0 = 3, P_d = 0.087 W/cm^3, d = 9.5 mm, and $C_{S(IV),0}$ = 2 mM).

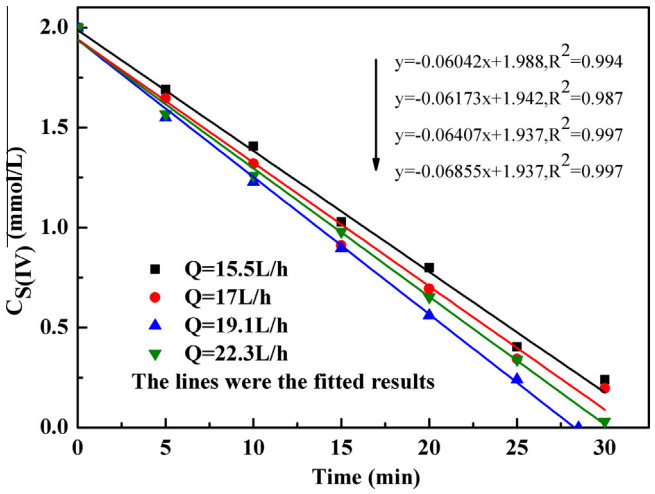

Fig. 10. Effect of effluent flow rate on oxidation rate (T = 283 K, pH_0 = 3, V_p = 15.9 - kV, and d = 9.5 mm).

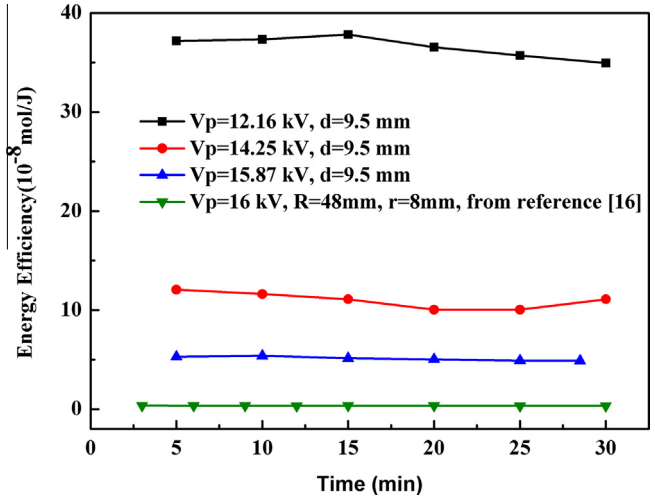

Fig. 11. Energy efficiency of S(IV) oxidation (T = 283 K, Q = 19.1 L/h, and pH_0 = 3).

In which, G is the energy efficiency of S(IV) oxidation, V_E is the effluent volume, t is the operation time and $C_{S(IV),t}$ is the corresponding S(IV) concentration.

Comparing Fig. 11 with Fig. 4a, it is found that though larger power density and electric field provide the higher oxidation rate, the energy efficiency is decreased. In addition, the energy efficiency of S(IV) oxidation by plate falling film discharge can be maintained on the order of 10^{-8} mol/J, however, the energy efficiency obtained in the cylindrical falling film discharge reactor is on the order of 10^{-9} mol/J [16]. Thus, the plate falling film discharge has an higher energy efficiency than cylindrical falling film discharge. This may be caused by the differences of power density and effective area of plasma between these two reactors. The power densities in the plate falling film discharge reactor and the cylindrical falling film discharge reactor are 0.11 W/cm^3 and 0.71 W/cm^3 respectively.

The effective area is defined as the surface area of falling film in plasma region divided by the volume of gaseous discharge plasma. Effective area of plate falling film discharge and cylindrical falling film discharge are calculated by the following equations:

$$S_p = \frac{S}{Sd} = \frac{1}{d} \quad (16)$$

$$S_c = \frac{2\pi r_o L}{\pi(r_o^2 - r_i^2)L} \approx \frac{2}{r_o}, \quad (r_i \ll r_o) \quad (17)$$

where S_p and S_c are effective area of plate falling film discharge and cylindrical falling film discharge respectively, r_o and r_i are inner radius of the outer tube and the HV electrode radius respectively, L is the length of the discharge gap.

The calculated effective area of the plate falling film discharge reactor and the cylindrical falling film discharge reactor are 1.05 cm^2/cm^3 and 0.83 cm^2/cm^3 respectively. The larger effective area and smaller power density of the plate falling film discharge reactor lead to the higher energy efficiency.

For industrial application, the surface of falling film must be enlarged. When increasing the surface area of plate falling film, the effective area is invariant. The energy efficiency can be maintained in a scale-up size plate falling film discharge reactor. While the effective area of cylindrical falling film decreases as the outer tube radius increases, which results in the decrease of energy efficiency. Thus, for a cylindrical falling film discharge reactor, the falling film surface can only be enlarged by prolonging the height of the reactor. However, the large height but small radius reactor is not desired in practical applications. Thus, the plate falling film discharge has the better potential for industrial application than cylindrical falling film discharge.

4. Conclusion

S(IV) oxidation can be enhanced by falling film discharge. The oxidation rate is determined by the discharge power density. The overall reaction is a combination of chain reaction path and radical self-reaction path, but the radical self-reaction path is dominating.

The actual kinetic equation of S(IV) oxidation by falling film discharge is complex and difficult to solve. Due to the linear relation between radical concentration and power density, the kinetic equation can be simplified in terms of S(IV) concentration and power density. The calculated reaction orders with respect to S(IV) and discharge power density are 0 and 0.75 respectively.

Compared with cylindrical falling film discharge, the plate falling film discharge has the better potential for larger scale application. Scale-up of a cylindrical falling film discharge reactor will decrease the energy efficiency while this efficiency can be maintained in a scale-up size plate falling film discharge reactor; thus, the plate falling film discharge would be more suitable for industrial application. This conclusion should be further confirmed by pilot scale comparison.

Acknowledgment

We appreciated the financial support to this study by National Natural Science Foundation of China (Nos. 20836008, 21076189, and U1162128).

References

[1] B.F. Vidal, P. Ollero, F.J. Gutierrez Ortiz, V. Villanueva, Catalytic seawater flue gas desulfurization process: an experimental pilot plant study, Environ. Sci. Technol. 41 (2007) 7114–7119.
[2] K. Oikawa, C. Yongsiri, K. Takeda, T. Harimoto, Seawater flue gas desulfurization: its technical implications and performance results, Environ. Prog. 22 (2003) 67–73.
[3] B.F. Vidal, P. Ollero, A kinetic study of the oxidation of S(IV) in seawater, Environ. Sci. Technol. 35 (2001) 2792–2796.
[4] B.F. Vidal, P. Ollero, F.J. Gutierrez Ortiz, R. Arjona, Catalytic oxidation of S(IV) in seawater slurries of activated carbon, Environ. Sci. Technol. 39 (2005) 5031–5036.
[5] K. Despina, P. Marina, L. Amedeo, Sulfite oxidation catalyzed by cobalt ions in flue gas desulfurization processes, J. Air Waste Manage. Assoc. 60 (2010) 675–680.

[6] L.D. Wang, Y. Zhao, Kinetics of sulfite oxidation in wet desulfurization with catalyst of organic acid, Chem. Eng. J. 136 (2008) 221–226.
[7] D.R. Grymonpre, W.C. Finney, R.J. Clark, B.R. Locke, Hybrid gas–liquid electrical discharge reactors for organic compound degradation, Ind. Eng. Chem. Res. 43 (2004) 1975–1989.
[8] P. Bruggeman, L. Graham, J. Degroote, J. Vierendeels, C. Leys, Water surface deformation in strong electrical fields and its influence on electrical breakdown in a metal pin–water electrode system, J. Phys. D: Appl. Phys. 40 (2007) 4779–4786.
[9] V.A. Titov, V.V. Rybkin, S.A. Smirnov, A.L. Kulentsan, H.-S. Choi, Experimental and theoretical studies on the characteristics of atmospheric pressure glow discharge with liquid cathode, Plasma Chem. Plasma Process. 26 (2006) 543–555.
[10] P. Bruggeman, P. Gusn, J. Degroote, J. Vierendeels, C. Leys, Influence of the water surface on the glow-to-spark transition in a metal-pin-to-water electrode system, Plasma Sources Sci. Technol. 17 (2008) 245014.
[11] P. Bruggeman, E. Ribezl, A. Maslani, J. Degroote, A. Malesevic, R. Rego, J. Vierendeels, C. Leys, Characteristics of atmospheric pressure air discharge with a liquid cathode and a metal anode, Plasma Sources Sci. Technol. 17 (2008) 025012.
[12] P. Bruggeman, J.V. Slychen, J. Degroote, J. Vierendeels, P. Verleysen, C. Leys, DC electrical breakdown in a metal pin–water electrode system, IEEE Trans. Plasma Sci. 36 (2008) 1138–1139.
[13] P. Bruggeman, J.J. Liu, Joris. Degroote, M.G. Kong, J. Vierendeels, C. Leys, DC excited glow discharge in atmospheric pressure air in pin-to-water electrode systems, J. Phys. D: Appl. Phys. 41 (2008) 215201.
[14] M. Sato, T. Tokutake, T. Ohshima, A.T. Sugiarto, Aqueous phenol decomposition by pulsed discharge on the water surface, IEEE Trans. Ind. Appl. 44 (2008) 1397–1402.
[15] B.P. Dojcinovic, G.M. Roglic, B.M. Obradovic, M.M. Kuraica, M.M. Kostic, J. Nesic, D.D. Manojlovic, Decolorization of reactive textile dyes using water falling film dielectric barrier discharge, J. Hazard. Mater. 192 (2011) 763–771.
[16] N. Shi, X.W. Zhang, L.C. Lei, Sulfite oxidation in seawater flue gas desulfurization by a pulsed corona discharge process, Sep. Purif. Technol. 70 (2009) 212–218.
[17] H.U. Sverdrup, M.W. Johnson, R.H. Fleming, The Oceans, Their Physics, Chemistry, and General Biology, Prentice-Hall, New York, 1942.
[18] G.V. Buxton, S. McGowan, G.A. Salmon, J.E. Williams, N.D. Wood, A study of the spectra and reactivity of oxysulphur-radical anions involved in the chain oxidation of S(IV): a pulse and γ-radiolysis study, Atmos. Environ. 30 (1996) 2483–2493.
[19] B. Eliasson, U. Kogelschatz, Nonequilibrium volume plasma chemical processing, IEEE Trans. Plasma Sci. 19 (1991) 1063–1077.
[20] B.R. Locke, A. Ichihashi, H.H. Kim, A. Mizuno, Diesel engine exhaust treatment with a pulsed streamer corona reactor equipped with reticulated vitreous carbon electrodes, IEEE Trans. Ind. Appl. 37 (2001) 715–723.
[21] P. Bruggeman, D. Schram, M.A. Gonzalez, R. Rego, M.G. Kong, C. Leys, Characterization of a direct DC-excited discharge in water by optical emission spectroscopy, Plasma Sources Sci. Technol. 18 (2009) 025017.
[22] R.N. Li, K.P. Yan, J.S. Miao, X.L. Wu, Heterogeneous reaction in non-thermal plasma flue gas desulfurization, Chem. Eng. Sci. 53 (1998) 1529–1540.
[23] K. Yan, E.J.M. van Heesch, A.J.M. Pemen, P.A.H.J. Huijbrechts, From chemical kinetics to streamer corona reactor and voltage pulse generator, Plasma Chem. Plasma Process. 21 (2001) 107–137.
[24] N. Sano, D. Yamamoto, T. Kanki, Decomposition of phenol in water by a cylindrical wetted-wall reactor using direct contact of gas corona discharge, Ind. Eng. Chem. Res. 42 (2003) 5423–5428.